**The EMBO Journal (2004) 23,** 2498–2509 | © 2004 European Molecular Biology Organization | All Rights Reserved 0261-4189/04
www.embojournal.org

THE EMBO JOURNAL

# Interactions between UvrA and UvrB: the role of UvrB's domain 2 in nucleotide excision repair

**James J Truglio[1,5], Deborah L Croteau[2,5], Milan Skorvaga[2,3,5], Matthew J DellaVecchia[2,5], Karsten Theis[1,4], Bhaskar S Mandavilli[2], Bennett Van Houten[2,*] and Caroline Kisker[1,*]**

[1]Department of Pharmacological Sciences, State University of New York at Stony Brook, Stony Brook, NY, USA, [2]Laboratory of Molecular Genetics, National Institute of Environmental Health Sciences, National Institutes of Health, Research Triangle Park, NC, USA, [3]Department of Molecular Genetics, Cancer Research Institute, Slovak Academy of Sciences, Bratislava, Slovakia and [4]Department of Biochemistry and Molecular Biology, University of Massachusetts Amherst, Amherst, MA, USA

**Nucleotide excision repair (NER) is a highly conserved DNA repair mechanism present in all kingdoms of life. UvrB is a central component of the bacterial NER system, participating in damage recognition, strand excision and repair synthesis. None of the three presently available crystal structures of UvrB has defined the structure of domain 2, which is critical for the interaction with UvrA. We have solved the crystal structure of the UvrB Y96A variant, which reveals a new fold for domain 2 and identifies highly conserved residues located on its surface. These residues are restricted to the face of UvrB important for DNA binding and may be critical for the interaction of UvrB with UvrA. We have mutated these residues to study their role in the incision reaction, formation of the pre-incision complex, destabilization of short duplex regions in DNA, binding to UvrA and ATP hydrolysis. Based on the structural and biochemical data, we conclude that domain 2 is required for a productive UvrA–UvrB interaction, which is a pre-requisite for all subsequent steps in nucleotide excision repair.**

*The EMBO Journal* (2004) **23,** 2498–2509. doi:10.1038/sj.emboj.7600263; Published online 10 June 2004
*Subject Categories*: structural biology; genome stability & dynamics
*Keywords*: crystallography; DNA damage; DNA repair nucleotide excision repair; UvrB

*Corresponding authors. C Kisker, Department of Pharmacological Sciences, State University of New York at Stony Brook, Stony Brook, NY 11794-5115, USA. Tel.: +1 631 632 1465; Fax: +1 631 632 1555; E-mail: kisker@pharm.sunysb.edu and B Van Houten, Laboratory of Molecular Genetics, National Institute of Environmental Health Sciences, National Institutes of Health, Research Triangle Park, NC 27709, USA. Tel.: +1 919 541 2799; E-mail: vanhout1@niehs.nih.gov
[5]These authors contributed equally to this work

**Received: 27 January 2004; accepted: 11 May 2004; published online: 10 June 2004**

## Introduction

Among the DNA repair mechanisms available to the cell, nucleotide excision repair (NER) stands out because of its broad substrate specificity (Van Houten, 1990; Friedberg *et al*, 1995; Lloyd and Van Houten, 1995; Sancar, 1996; Goosen and Moolenaar, 2001). This repair mechanism is unique in its versatility to repair substrates, including carcinogenic cyclobutane pyrimidine dimers induced by UV radiation, benzo[*a*]pyrene-guanine adducts caused by smoking and guanine-cisplatinum adducts formed during chemotherapy (Sancar, 1994). NER in bacteria, one of the first repair mechanisms discovered (Boyce and Howard-Flanders, 1964; Setlow and Carrier, 1964), is mediated by the products of the *uvrA*, *uvrB* and *uvrC* genes. UvrA is involved in damage recognition and was generally believed to form a heterotrimeric ($UvrA_2UvrB$) complex with UvrB (Theis *et al*, 2000). Recently, however, the formation of a heterotetrameric ($UvrA_2UvrB_2$) complex was suggested (Verhoeven *et al*, 2002). The UvrAUvrB complex has helicase-like properties and specifically identifies conformational perturbations induced by DNA lesions (Oh and Grossman, 1987, 1989; Koo *et al*, 1991). After the damage has been identified, UvrA dissociates, while UvrB remains bound to the DNA in a stable pre-incision complex (Orren and Sancar, 1990). UvrC binds to this complex and mediates the incision four nucleotides 3′ of the damaged site, followed by an incision seven nucleotides 5′ of the damaged site (Sancar and Rupp, 1983; Lin and Sancar, 1992; Lin *et al*, 1992; Verhoeven *et al*, 2000). UvrD and DNA polymerase I are required for turnover of the UvrABC proteins (Caron *et al*, 1985; Husain *et al*, 1985). UvrD removes UvrC and the oligonucleotide containing the lesion, while UvrB remains bound to the gapped DNA until it is filled by DNA polymerase I (Husain *et al*, 1985). The reaction is completed by DNA ligase, closing the nicked DNA. This multi-step process of DNA recognition and repair ensures discrimination between damaged and nondamaged DNA.

UvrB plays a central role in this repair cascade. It forms a productive complex with UvrA that recognizes the damage and guides the DNA from recognition to incision by complex formation with UvrC. Finally, it is involved in repair synthesis, ensuring that no gapped DNA intermediates are released before the repair pathway is completed. Sequence analysis of UvrB revealed that residues 154–251 share homology with the transcription repair-coupling factor Mfd. Since both Mfd and UvrB interact with UvrA, it was proposed that these homologous regions are involved in interactions with UvrA (Selby and Sancar, 1993). Biochemical studies using either residues 115–250 or the C-terminal residues 547–673 of *Escherichia coli* UvrB fused to a maltose-binding protein suggest that the first region interacts specifically with UvrA and the C-terminal region interacts with UvrA and UvrC (Hsu *et al*, 1995). Both interactions are salt-dependent, indicating that ionic interactions are important for UvrAUvrB complex formation.

 

We solved the three-dimensional structure of the *Bacillus caldotenax* UvrB variant Y96A. Despite the presence of three independently determined UvrB structures (Machius *et al*, 1999; Nakagawa *et al*, 1999; Theis *et al*, 1999), no structural information was obtained with respect to the putative UvrA-interacting domains. The 60 C-terminal amino acids as well as domain 2 harboring residues 151–251 are highly flexible in all three structures. The structure of the C-terminal domain was solved independently, revealing a coiled coil conformation (Sohi *et al*, 2000; Alexandrovich *et al*, 2001). Domain 2 was partially modeled as a poly-alanine model in two of the three structures (Nakagawa *et al*, 1999; Theis *et al*, 1999), although the structural details of this domain have remained elusive. The structure of the Y96A variant allowed, for the first time, a detailed atomic analysis of domain 2. We identified several highly conserved residues on the surface of this domain, which may be critical for the interaction with UvrA. These residues define a patch that is located in close proximity to the proposed DNA-binding site of UvrB. Analyses of mutants within this patch support the conclusion that the crosstalk between UvrA and UvrB, leading to damage recognition, requires UvrA-interacting residues on the surface of domain 2 of UvrB. These interactions are critical since the formation of a productive complex allows damage recognition and repair, the first step in the reaction cascade of NER.

## Results

### *Structure of the Y96A variant*

The crystal structure of the UvrB Y96A variant from *B. caldotenax* was solved by molecular replacement using the wild-type (WT) structure (PDB code 1D9X) as a search model. The protein crystallized in space group $P3_221$ with two molecules in the asymmetric unit, which are related to each other by a translation of ~0.5 along the *z*-axis. This is in contrast to WT UvrB, which crystallizes in space group $P3_121$ and contains a single molecule in the asymmetric unit (Theis *et al*, 1999). In both structures, the functional unit of the protein is a monomer. The structure was refined at 2.6 Å resolution to an *R* factor of 0.230 and $R_{free}$ of 0.286 (Table I). The two Y96A molecules have nearly identical conformations, with r.m.s. deviations of 0.92 Å for all Cα atoms.

### *Structure of domain 2*

In all the three UvrB structures that have been described so far (Nakagawa *et al*, 1997, 1999; Machius *et al*, 1999; Theis *et al*, 1999), it was not possible to define domain 2 presumably due to disorder. Unexpectedly, the new crystal form of the Y96A mutant provided well-defined electron density for domain 2 due to more favorable crystal packing. The structure of domain 2 of UvrB has a βαββββββββ topology (Figures 1 and 2B). The core of the domain is formed by a twisted six-stranded antiparallel meander β sheet formed by β strands β2–β7. One side of this β sheet faces the solvent, while the other side interacts with an α helix (α1) and a two-stranded antiparallel β sheet consisting of β1 and β8. The α helix runs parallel to the six-stranded β sheet and makes contacts to the first three strands of the sheet (β2–β4), while its fourth and fifth strands, β5 and β6, interact predominantly with the two-stranded β sheet. The sixth strand is a solvent exposed on both sides. Topology analysis with Dali (Holm and Sander, 1995) failed to identify related structures in the Protein Data Bank. This new protein fold only contains sequence homology to Mfd (Figure 2B, lower panel), the bacterial transcription repair-coupling factor, which is functionally similar to UvrB in its ability to bind to UvrA.

**Table I** Data collection and refinement statistics

| | Native |
|---|---|
| *Data collection* | |
| Space group | $P3_221$ |
| Unit cell dimensions | |
| *a*, *b*, *c* (Å) | 150.8, 150.8, 159.8 |
| α, β, γ (deg) | 90.0, 90.0, 120.0 |
| Resolution limits (Å) | 30.0–2.6 Å |
| Completeness (%) | 99.9 |
| $R_{sym}$ | 0.073 (0.506) |
| $\langle I\rangle/\langle\sigma I\rangle$ | 17.5 (2.2) |
| *Refinement statistics* | |
| Number of observed reflections | 417 520 |
| Number of unique reflections | 61 397 |
| Number of protein/cofactor atoms | 9680 |
| Number of waters | 228 |
| $R_{cryst}$ ($R_{free}$) | 0.230 (0.286) |
| Deviations from ideal values in | |
| Bond lengths (Å) | 0.020 |
| Bond angle distances (deg) | 1.9 |
| Ramachandran statistics | 90.1/9.4/0.5/0.0 |

$R_{sym} = \sum_{hkl}\sum_i|I_i - \langle I\rangle|/\sum_{hkl}\sum_i\langle I\rangle$ where $I_i$ is the *i*th measurement and $\langle I\rangle$ is the weighted mean of all measurements of *I*. $\langle I\rangle/\langle\sigma I\rangle$ indicates the average of the intensity divided by its average standard deviation. Numbers in parentheses refer to the respective highest resolution data shell in each data set. $R_{cryst} = \sum||F_0| - |F_c||/|F_0|$, where $F_0$ and $F_c$ are the observed and calculated structure factor amplitudes. $R_{free}$ same as $R_{cryst}$ for 5% of the data randomly omitted from the refinement. Ramachandran statistics indicate the fraction of residues in the most favored, additionally allowed, generously allowed and disallowed regions of the Ramachandran diagram, as defined by the program PROCHECK.

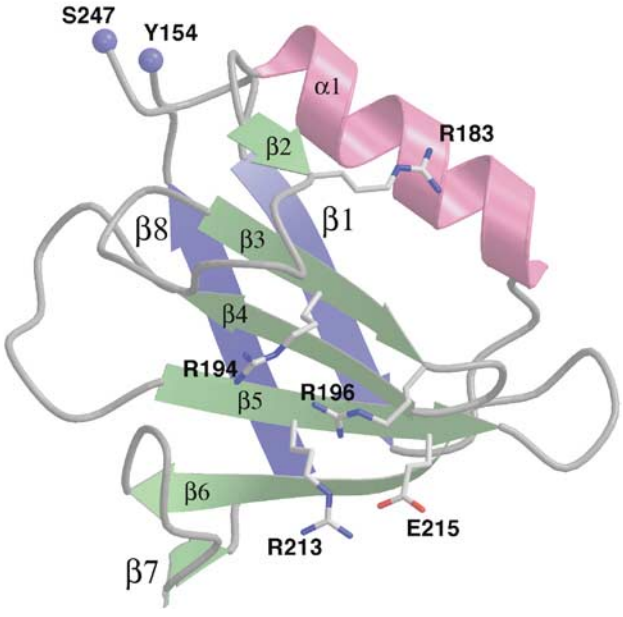


**Figure 1** Three-dimensional structure of the UvrA-interacting domain (domain 2) of UvrB. The ribbon diagram shows the secondary structure elements and mutated residues on the proposed UvrA interacting face. The core β sheet (β2–β7) is shown in green, a second sheet in blue (β1, β8) and the single α helix in pink. Blue spheres as well as residue labels mark the beginning and end of domain 2.

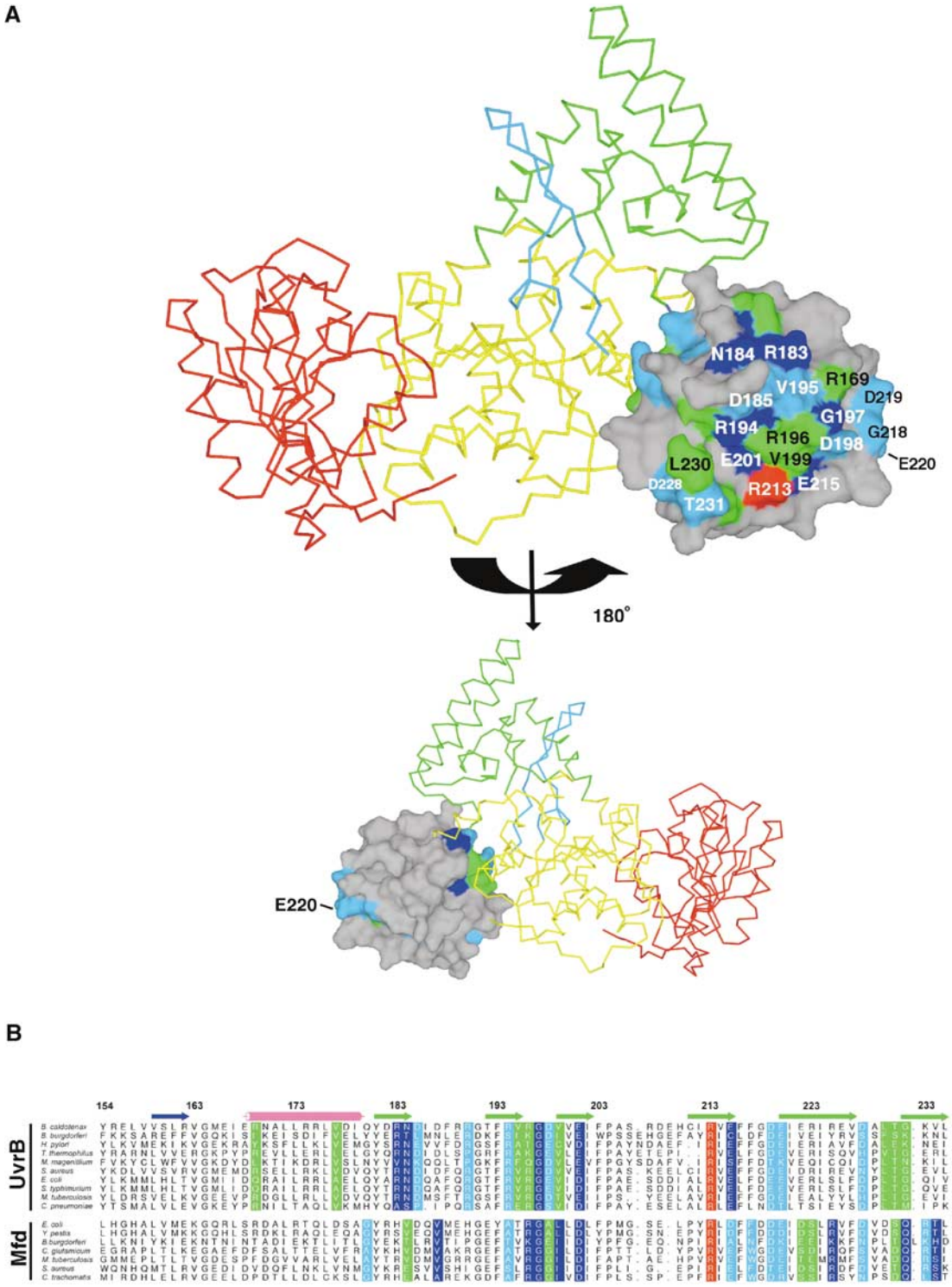


**Figure 2** Sequence conservation of domain 2 in UvrB. (**A**) Surface representation of domain 2 of UvrB (gray) with conserved residues labeled and color-coded (red: strictly conserved, dark blue: very highly conserved, cyan: highly conserved, green: moderate to highly conserved). Conservation is based on 56 domain 2 sequences aligned using ClustalX and analyzed by the ConSurf server. The upper panel shows the front (DNA-binding) side of UvrB and the lower panel is a 180° rotation showing the back. The remainder of UvrB is drawn as a Cα trace and color-coded according to domain architecture with domain 1a in yellow, 1b in green, 3 in red and the β hairpin in cyan. (**B**) Sequence alignment of UvrB domain 2 (first block) and the homologous domain in Mfd (second block). UvrB sequences from *Bacillus burgdorferi* (gi:8134783), *Helicobacter pylori* (gi:15645728), *T. thermophilus* (gi:2499102), *Mycoplasma genitalium* (gi:12044925), *Staphylococcus aureus* subsp. aureus MW2 (gi:21282449), *E. coli* (gi 137190), *Salmonella typhimurium* species LT2 (gi 16764161) and *Mycobacterium tuberculosis* (gi 3122992), and Mfd sequences from *E. coli* strain 0157:H7 (gi:15830746), *Yersinia pestis* (gi:16121893), *B. burgdorferi* (gi:3914012), *Corynebacterium glutamicum* species ATCC 13032 (gi:41325189), *M. tuberculosis* species H37Rv (gi:15608160), *S. aureus* subsp. aureus N315 (gi:15926180) and *Chlamydia trachomatis* (gi:15605481) are included. The secondary structure is indicated above the sequence with arrows for β-strands and a cylinder for the α-helix. Color coding of secondary structure was chosen to match that of Figure 1. Residues are highlighted according to the conservation shown in (A).

### *Interactions between domain 2 and the remainder of UvrB*

Domain 2 is built by a continuous stretch in the polypeptide and connects domain 1a with domain 1b (Figure 2A). Apart from these covalent connections, most of the interdomain interactions involve an α helix C terminal to the β hairpin of domain 1a, which encompasses residues 117–131 (helix 1a-α4; Figure 3A), and mostly residues located in loop regions of domain 2. Residues Phe 131 and His 124 at the C-terminal half of the helix along with residue Tyr 328 form hydrophobic and stacking interactions with residues His 248, Tyr 154 and Pro 245. The hydrophobic core extends to residues Val 250, Leu 157 and Ile 179. The center of helix 1a-α4 comes in close contact to the main chain atoms of domain 2 (the distance

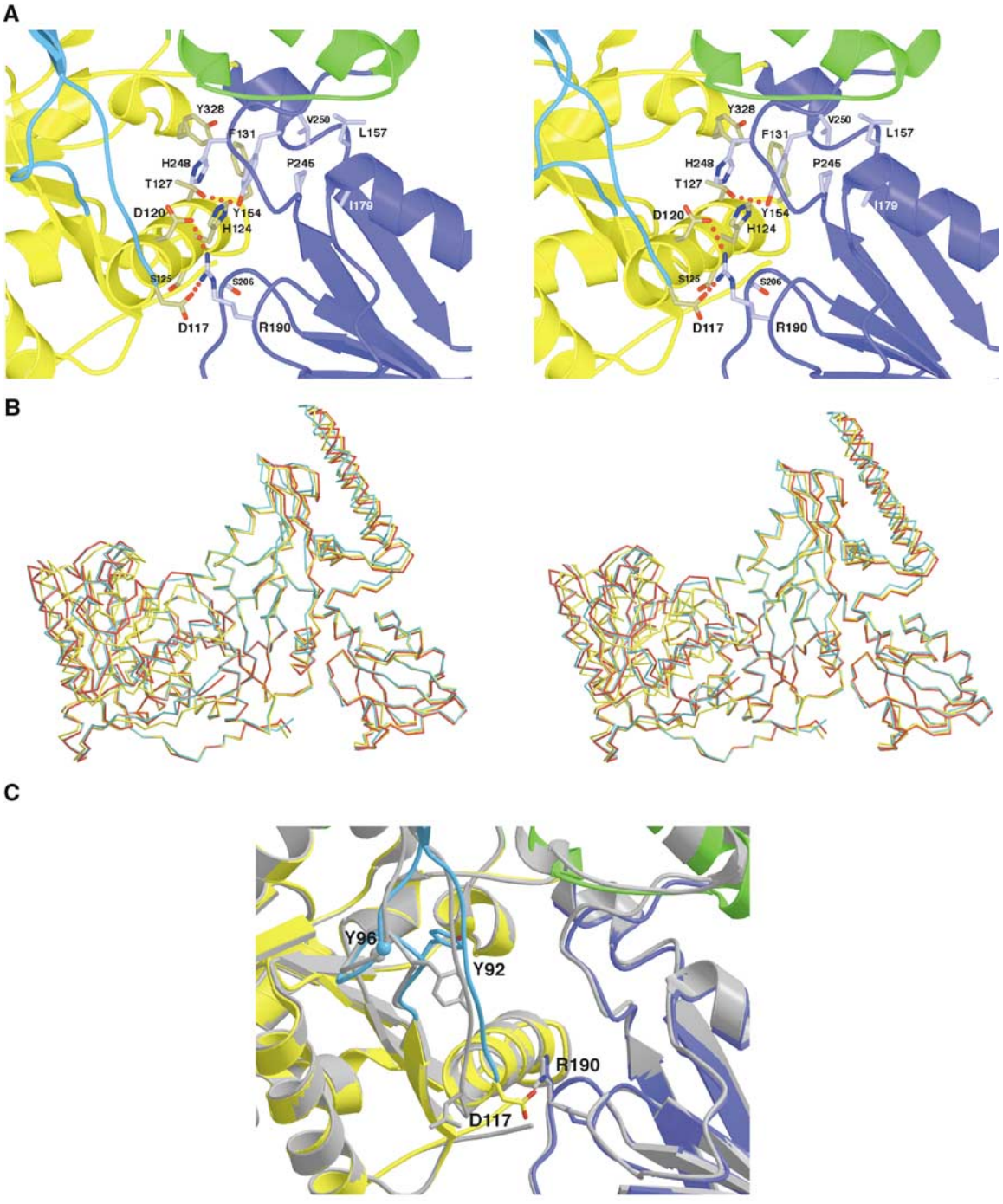


**Figure 3** Comparison of the Y96A UvrB structure to WT UvrB. (**A**) Stereo view of the interface between domain 2 and the remainder of the UvrB molecule. Selected side chains are shown and labeled. Color coding is according to domain architecture as in Figure 2A and domain 2 in blue. Hydrogen bonds and salt bridges are indicated by red dotted lines. (**B**) Comparison of the overall structure of WT UvrB (cyan) and the two NCS-related copies of UvrB Y96A (yellow and red) as a stereo view. Orientation is chosen as in Figure 2. For the superposition, domain 1a of each of the structures was used and the resulting transformations were applied to the entire molecule. (**C**) Superposition of UvrB Y96A (color coded as in Figure 2) and WT UvrB (gray). Side chains for Tyr 92, Asp 117 and Arg 190 are shown for both the WT and the UvrB Y96A structure. The side chain of Y96 is omitted from the native model since the electron density for this residue is insufficient. A sphere indicates the position of the Cα atom of Y96 (A96 for the mutant).

between the Cα atom of residue 125 and the Cβ atom of residue 206 is 3.7 Å). Two aspartate side chains from the N-terminal part of helix 1a-α4, Asp 117 and Asp 120 form salt bridges to Arg 190 of domain 2. Comparing the sequences of *B. caldotenax* and *Thermus thermophilus*, Arg 190 is not conserved in *T. thermophilus*, but replaced by Pro 187. Likewise, Pro 114 from *T. thermophilus* replaces Asp 117. Although domain 2 was resolved only partially in the structure of *T. thermophilus* UvrB solved by Nakagawa *et al* (1999), the fragment of domain 2 that interacts with domain 1 was included in their model. Pro 114 and Pro 187 are observed in van der Waals contact to each other, but this interaction does not lead to a closer approach of domain 2 to domain 1a compared to the UvrB *B. caldotenax* structure.

### *Structural variation between WT UvrB and the Y96A variant*

After retracing and completing the model of domain 2 based on the Y96A diffraction data, we re-examined the WT data and model (Theis *et al*, 1999). The completed model of domain 2 obtained from the Y96A mutant was placed into the WT model. The refinement of the corrected WT model against the original diffraction data did not improve the density or the $R_{free}$. Presumably, this is because domain 2 has a large range of motion in the WT crystal form and there is very little density in this region. We compared the overall structures of WT UvrB and the Y96A variant. Separate superpositions of single domains show that there is little change within the domains (1a: 0.66 Å; 1b: 1.1 Å; 2: 0.46 Å; 3: 0.41 Å r.m.s. deviations between corresponding Cα atoms). However, after superimposing residues of domain 1a only, comparison of the entire structure shows some variations in the orientation of the individual domains (Figure 3B). Similar to the results when UvrB structures from different organisms were compared (Theis *et al*, 2000), domain 3 and domain 1b along with the tip of the β hairpin change their orientation with respect to domain 1a. Apart from these domain motions, local structural differences between the WT and the Y96A variant are observed near the mutation in the β hairpin and in helix 1a-α4 C terminal to the β hairpin. Upon mutation of Tyr 96 to alanine, the side chain of Tyr 92 changes its position and forms a hydrogen bond to the backbone carbonyl group of residues Lys 111 and Ala 113 on the opposite side of the β hairpin (Figure 3C). This conformational change may stabilize the N-terminus of helix 1a-α4 including Asp 117, and in turn stabilizes the interaction between Asp 117 and Arg 190 (Figure 3A). In WT UvrB, helix 1a-α4 is frayed at its N terminal, resulting in a conformation of Asp 117 that points away from Arg 190 and prevents formation of the salt bridge observed in the structure of the Y96A variant (Figure 3C). Thus, comparison of the structures of the Y96A variant and WT UvrB suggests how a change in the conformation of the β hairpin might influence the interaction of domain 1a with domain 2. The other interactions observed between domain 2 and the remainder of UvrB are unchanged between WT and the Y96A variant.

### *Sequence conservation*

In order to locate the UvrA-interaction interface on domain 2, we mapped the sequence conservation of domain 2 of UvrB from different organisms onto the surface (Figure 2A). The sequence alignment for a randomly selected subset of these organisms is shown in Figure 2B (upper panel). The only solvent-exposed residue of domain 2 that is strictly conserved is Arg 213, which is part of β strand β5 located at the center of the six-stranded sheet. This arginine is also strictly conserved in the homologous domain of Mfd (Figure 2B), which interacts with UvrA as well. To quantify the level of conservation of the other residues, we used the ConSurf server, which bases conservation scores of single-residue positions on phylogenetic trees calculated for the whole sequence.

The highly conserved and functionally important residues of UvrB, including the ATPase active site and the β-hairpin structure involved in DNA binding, are clustered on one face of the molecule. The location of conserved surface residues in domain 2 of UvrB follows this pattern, with a front side (Figure 2A, upper panel) that contains highly conserved patches and a backside (Figure 2A, lower panel) lacking conservation. The largest conserved patch consists of a band of residues including the strictly conserved Arg 213, with Asp 228 on one end and Glu 220 on the other end. Some of the conserved surface residues are hydrophobic (i.e. Leu 230), but most of the conserved residues are charged. Calculation of the electrostatic potential showed neither predominantly negative nor positive charged patches. Instead, there is a pattern of positively charged residues, mostly arginines, interspersed with the negatively charged glutamates and aspartates, resulting in a net charge of zero.

### *Point mutants*

The interaction between UvrA and domain 2 was shown to be salt-labile, suggesting mostly electrostatic interactions (Hsu *et al*, 1995). We therefore targeted charged residues as candidates for single or double mutants in an attempt to identify residues in domain 2 that are critical for the interaction with UvrA. We analyzed the point mutant R183E and three double mutants R194A/R196A, R194E/R196E and R213A/E215A (Figure 1). The R213A/E215A mutant changes the strictly conserved Arg 213 without affecting the net charge of the protein, because the nearby Glu 215 is mutated to alanine as well. Arg 183 is conserved in UvrB. The R183E and R194A/R196A, and R194E/R196E mutants decrease the net charge of domain 2 by two and four units, respectively, which is expected to affect the electrostatic interactions with UvrA to different degrees.

### *DNA incision activity of UvrB domain 2 mutants*

We first investigated the ability of the mutants to function in the DNA incision assay. Using a model substrate of a 50 bp duplexed DNA containing a single fluorescein-adducted thymine (FldT), we determined that the incision activity for the mutants varied significantly. The most severely compromised UvrB mutant is the protein that lacks domain 2 entirely, the Δ2 mutant. Little, if any, incision activity was detected when this domain was deleted (Figure 4). Folding of this mutant was confirmed by circular dichroism experiments (data not shown). Upon our initial evaluation of the domain 2 point variants, no significant differences were observed in the incision assay compared to the WT protein (Figure 4D, 30 min). However, significant differences between WT UvrB and domain 2 variants were apparent at shorter incubation intervals. The double mutants R194A/R196A and R213A/E215A display similar incision activities compared to WT UvrB when using FldT as the substrate. The remaining two

 

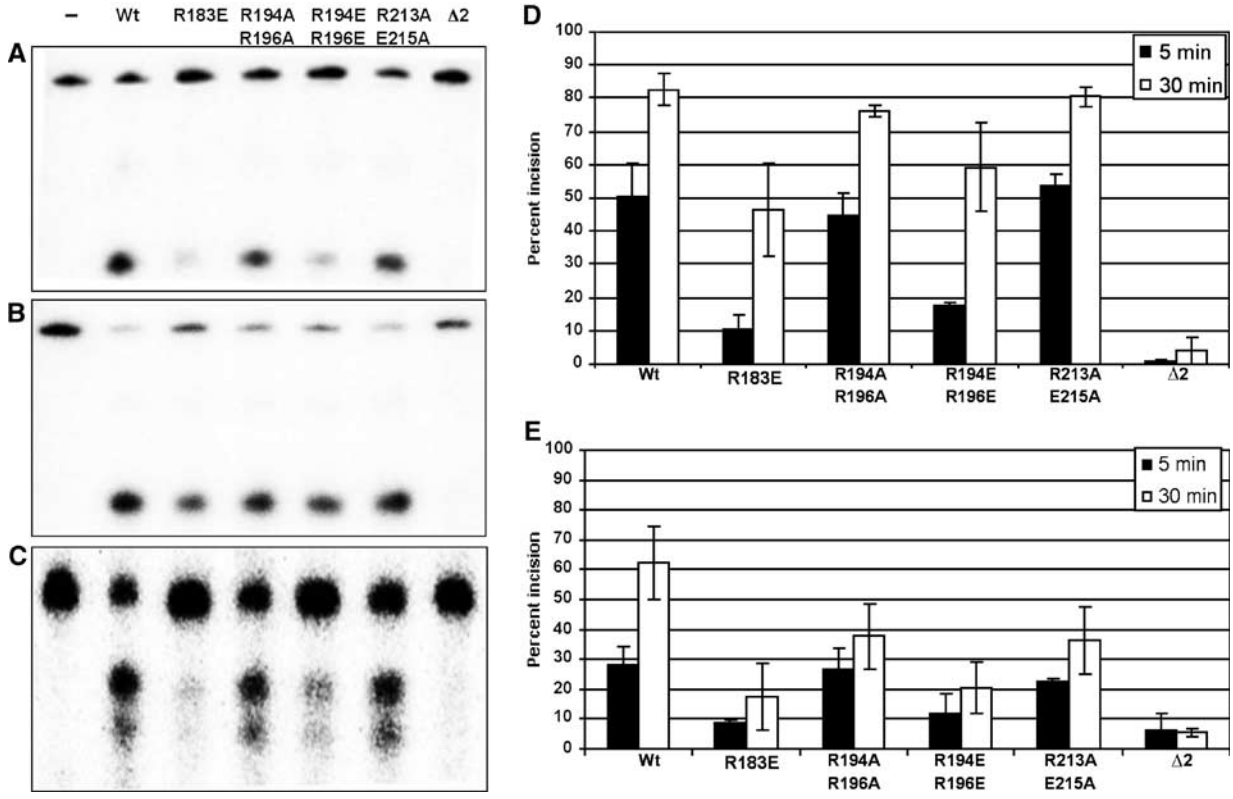


**Figure 4** Incision activity of domain 2 mutants. (**A, B, C**): The 5′-end-labeled substrate was incubated with 20 nM UvrA, 50 nM UvrC and 100 nM of the indicated UvrB protein for 5 min (A) or 30 min (B, C), at 55°C in reaction buffer. The reactions were terminated with stop buffer, and the incision products were analyzed on a 10% denaturing polyacrylamide gel. (**D, E**): Comparison of the incision activity at 5 min (black bars) and 30 min (white bars) using the indicated UvrB proteins. Data are reported as the mean ± the standard deviation of the mean of two to four incision assays per time point and substrate. Panels A, B and D: 50 mer dsDNA substrate containing a centrally located fluorescein (FldT). Panels C and E: 50 mer dsDNA substrate containing a centrally located single-nucleotide gap.

mutants, R183E and R194E/R196E, possess significantly lower activities than WT UvrB, with 10 and 18%, compared to 50% of the substrate incised, respectively.

Since the UvrABC system repairs many different DNA lesions varying in size and structure, we analyzed the UvrB mutants on a second DNA substrate to determine if the mutations affect only bulky substrates or lead to additional defects not seen with the FldT substrate. We therefore chose to evaluate the incision activity on a gapped heteroduplex containing a single-nucleotide gap with a 3′-hydroxyl and a 5′-phosphate at the gap. The overall incision activity for all proteins tested is reduced relative to that seen with the FldT substrate (Figure 4C and E) and the Δ2 UvrB mutant is again catalytically inactive. Curiously, with this substrate two of the mutants, R194A/R196A and R213A/E215A, appeared to have near WT levels of incision at the 5 min time point (25, 22 and 27% substrate incised, respectively), but failed to achieve the full level of activity of the WT protein within 30 min (38, 35 and 60% substrate incised, respectively). The second substrate clearly shows that the R183E and R194E/R196E mutants are severely compromised in the incision assay (5 min, 9 and 12%; 30 min, 17 and 21%).

### *UvrA–UvrB protein–protein interaction*

One possibility why the UvrB mutant proteins fail to incise the DNA substrates to the same extent as WT UvrB may be due to impaired protein–protein interactions between UvrA and UvrB. To directly test whether UvrA is interacting with UvrB, we performed a pull-down assay. We overexpressed the *B. caldotenax* UvrA-chitin-binding domain fusion protein (UvrA–CBD) in *E. coli*, and bound the UvrA–CBD protein to chitin resin. The resin-bound UvrA was washed and then incubated with different UvrB proteins. Figure 5 shows the proteins that remain bound to the beads after they have been washed. Even though ~7 μg of UvrA were bound to the chitin beads, nonspecific binding by BSA was not detected (panel C, lane 2). Both WT UvrB and the Δβ-hairpin mutant possess an intact domain 2 and are readily retained. In contrast, the Δ2 UvrB mutant is not retained at all. Mutants R183E and R194E/R196E are retained by the UvrA beads to only 10 and 5% of WT UvrB, respectively, while mutants R194A/R196A and R213A/E215A are bound at about 40 and 12%, respectively. The decrease of incision by these mutants can be attributed to UvrA's reduced ability to recruit these UvrB proteins.

### *Loading of UvrB domain 2 mutants onto DNA*

While the pull-down assay demonstrates that all UvrB domain 2 mutants show impaired UvrA binding in the absence of DNA, the relative affinity of UvrA for UvrB may be altered in the presence of substrate DNA. In the course of the UvrABC incision reaction, several of the protein–DNA intermediates are sufficiently stable to be visualized on a native gel: (1) $UvrA_2$–DNA, (2) UvrAUvrB–DNA and (3) UvrB–DNA

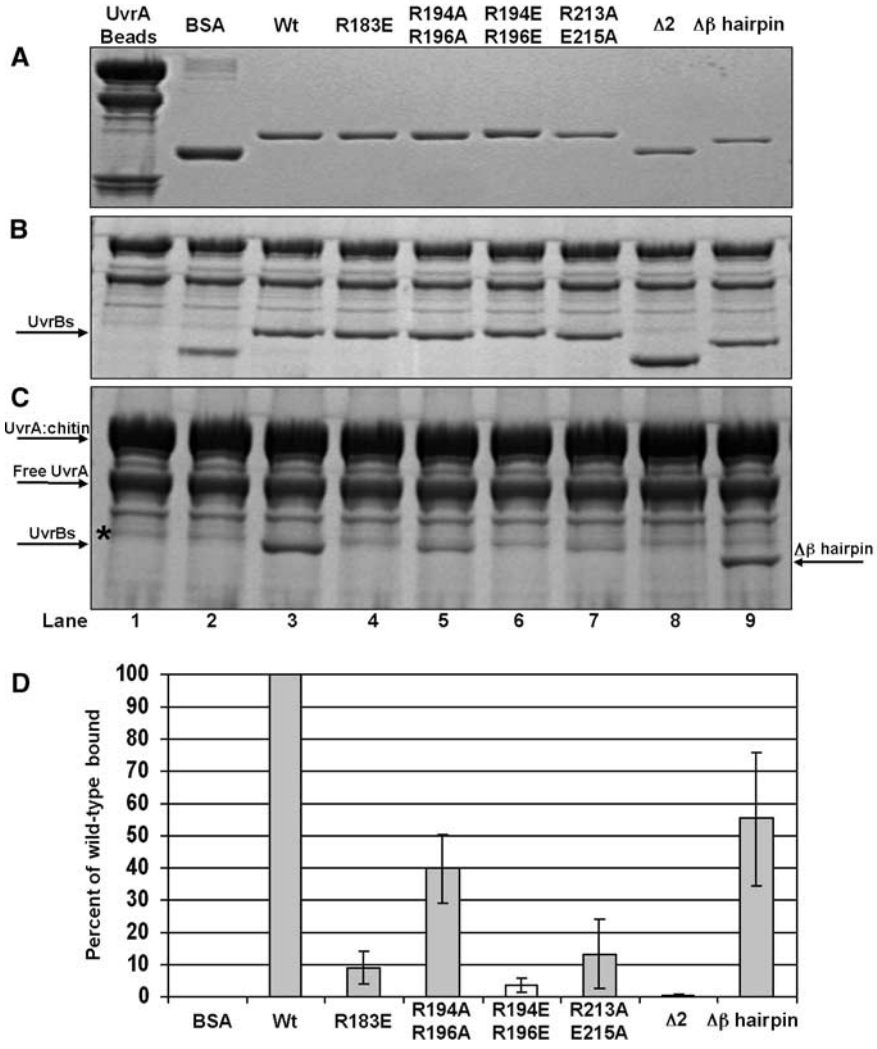


**Figure 5** UvrA pull-down assay. The UvrA-chitin beads were incubated with either WT UvrB or the mutants. After washing the beads extensively, the bound proteins were analyzed on a 10% denaturing polyacrylamide gel. (**A**) Sample of all proteins used in the study. (**B**) One-twentieth of the reactions, the 'inputs'. (**C**) Proteins that remained bound to the resin after extensive washing. (**D**) Quantitation of panel C reporting the percent of WT UvrB bound (data reported as the mean ± the standard error of the mean $n = 2$). The asterisk (*) in panel C, lane 1 indicates a nonspecific band observed in all reaction lanes, which migrates just above the band for UvrB. For quantitation, the area of this band was subtracted from all lanes except Δ2 and Δβ hairpin, whose proteins migrate faster.

complexes (Zou *et al*, 1995). We employed a gel mobility shift assay to evaluate how well the UvrB mutants are able to generate the different complexes. In addition, we determined how readily the various UvrB mutants are able to form productive interactions with UvrA by the appearance of the UvrB–DNA intermediate.

We tested complex formation after 5 and 20 min of incubation to detect minor differences between the mutants (Figure 6A and B, respectively). In the absence of UvrB, UvrA forms a weak complex with the DNA, observed as a slowly migrating species containing 6% of the total DNA. Upon adding WT UvrB, an additional species with intermediate mobility appears (amounting to 60% of total DNA at both time points) corresponding to the UvrB–DNA complex. Moreover, the slowly migrating band increases to about 14% of total DNA in the presence of UvrB. Previous experiments have shown that this band contains two species with very similar mobilities, the UvrA–DNA and UvrAUvrB–DNA complexes; however, for the Δβ-hairpin mutant the UvrAUvrB–DNA complex has a clearly distinguishable mobility compared to the UvrA–DNA complex (Skorvaga *et al*, 2002; Figure 6A, lanes 2 and 9), presumably because altering the β hairpin results in a distinct protein–DNA complex.

The amount of the pre-incision complex formed with the different domain 2 mutants varies considerably. Amounts similar to those observed for WT UvrB (60%) after 20 min incubation are detected for R194A/R196A (61%) and R213A/E215A (58%), near WT amounts for R194E/R196E (47%) and lower amounts for R183E (27%) and the Δ2 mutant (not detectable). Mutants R194E/R196E and R183E show an approximately two-fold increase in the amount of pre-incision complex formed at 20 min compared to 5 min (47 versus 22% and 27 versus 13%, respectively), consistent with large differences observed for the FldT incision activity at two different incubation times; suggesting that these mutations slow down the formation of the damage recognition complex.

 

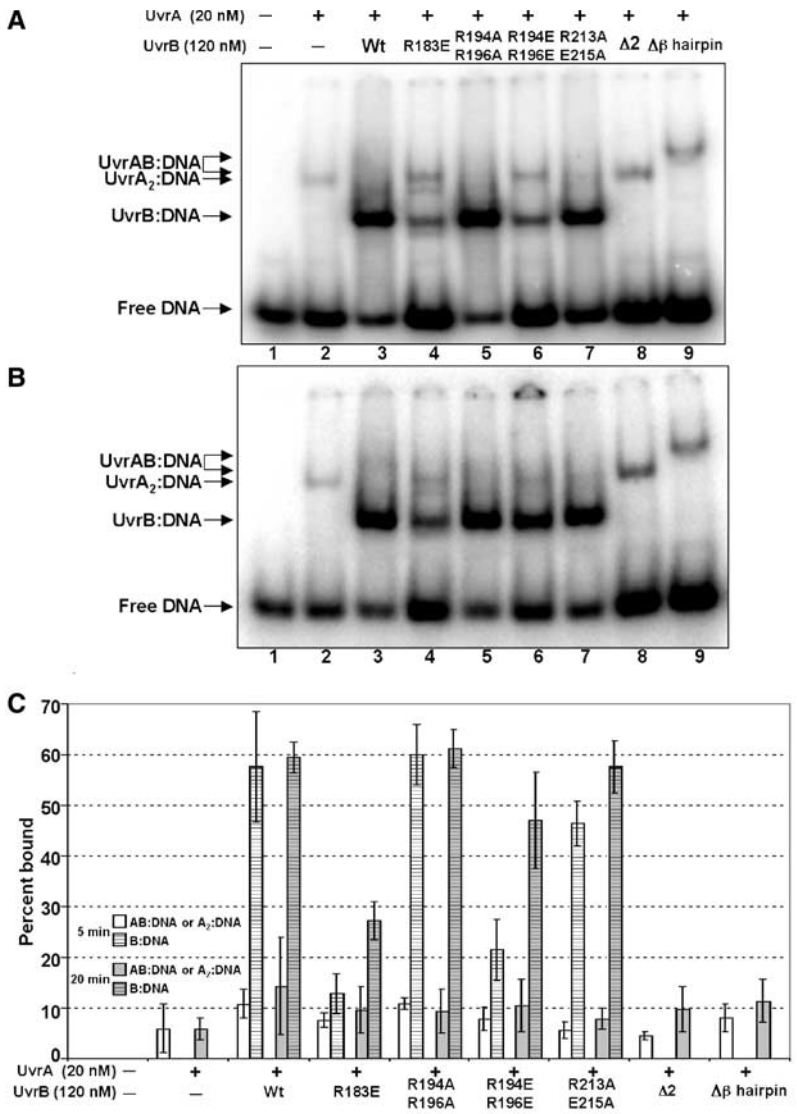


**Figure 6** Protein–DNA complex formations by UvrA and WT UvrB or UvrB mutants. UvrA (20 nM) was incubated with the various UvrB proteins (120 nM) as indicated at 55°C for 5 min (**A**) or 20 min (**B**) in the presence of 2 nM $F_{26}$, 50 duplex DNA with the modified strand 5′ terminally labeled. The reaction mixtures were analyzed on 4% polyacrylamide native gels in the presence of 1 mM ATP and 10 mM $MgCl_2$. (**C**) Quantitation of EMSAs in panels A and B, reporting the percent of DNA bound to UvrA, WT UvrB or UvrB mutants at 5 and 20 min (data are reported as the mean ± the standard deviation ($n = 3$) for each time point). White bars (solid or striped) indicate the percentage of DNA bound as the AB:DNA/$A_2$:DNA or B:DNA complexes, respectively, at 5 min. Gray bars (solid or striped) indicate the percentage of DNA bound at 20 min.

### *Oligonucleotide-destabilizing activity of UvrB domain 2 mutants*

The ability of the UvrAUvrB complex to locally unwind DNA in the vicinity of the damage is critical for UvrB's role in the damage recognition/confirmation process (Skorvaga *et al*, 2002), and we therefore analyzed whether the mutants still support separation of double-stranded DNA (Figure 7). Consistent with the previous assays, the Δ2 UvrB protein is catalytically inactive. The R194A/R196A and R213A/E215A mutants display 37 and 48% reductions in activity, respectively, at 10 min and barely significant differences compared to WT UvrB at 30 min. The remaining two mutants, R183E and R194E/R196E, have a reduced activity at both time points, showing 73 and 51% reductions in activity at 30 min, respectively.

### *Effects of domain 2 mutations on ATPase/GTPase activity*

ATP binding and hydrolysis is required for the UvrABC system to function (Oh and Grossman, 1987). As shown above, the various UvrB mutants displayed different DNA incision, complex formation and oligonucleotide-destabilizing activities compared to WT UvrB. Each of these steps is believed to require ATP binding, hydrolysis or both. To test whether specific mutations within domain 2 of the UvrB protein result in altered ATP binding and/or hydrolysis by UvrB, we measured the UV-irradiated damaged DNA (UV-DNA) activation of the UvrAUvrB complex ATPase. To distinguish the activity contributed by each protein in the UvrAUvrB complex, this experiment was repeated in the presence of GTP, since UvrA can utilize both ATP and GTP

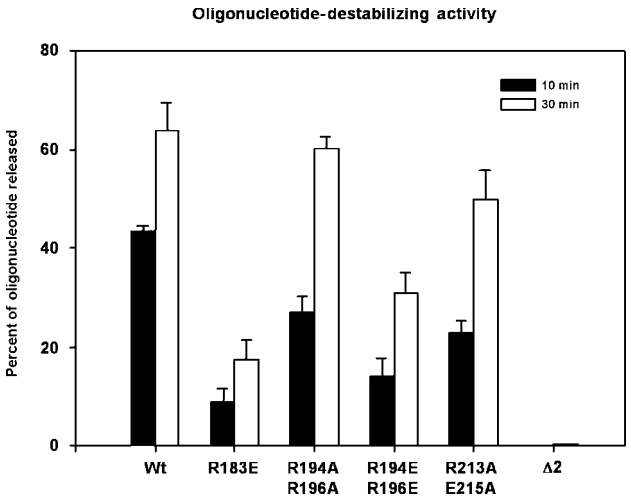


**Figure 7** Oligonucleotide-destabilizing activity of domain 2 mutants. The helicase substrate M13-F26/M13mp19(+)(8 fmol) was incubated with UvrA (50 nM) and UvrB WT or mutant (100 nM) at 42°C for 10 (black bars) or 30 min (white bars) ($n$ = mean of three, ±s.d.).

while UvrB specifically utilizes ATP (Thiagalingam and Grossman, 1993).

In the presence of damaged DNA, UvrA exhibits similar levels of ATPase and GTPase activity, whereas the ATPase activity of WT UvrB by itself is barely above background (Figure 8). When UvrA and UvrB are combined in the presence of damaged DNA, an increase in ATPase activity is observed compared to UvrA's activity. Since UvrA's GTPase activity does not increase under similar conditions, this increase in ATPase activity can be attributed to UvrB's cryptic ATPase activity, which is unlocked in the presence of UvrA, specifically in the UvrAUvrB damage recognition complex.

All domain 2 mutants, except the R194E/R196E mutant, tested in a UvrA/UvrB/UV-DNA reaction displayed ATPase activities slightly higher than those observed for UvrA/UV-DNA only, but much lower than the ATPase activity observed in the presence of WT UvrB. The R194E/R196E mutant shows ATPase activity similar to UvrA/UV-DNA only. In addition, all domain 2 mutants demonstrate an elevated GTPase activity of UvrA in the presence of UV-DNA. The ATPase data show that for the domain 2 mutants, UvrB's ATPase activity appears to be muted in the presence of UvrA and UV-DNA. UvrA in the presence of the Δβ-hairpin mutant and UV-DNA exhibited a lower GTPase activity than UvrA/UV-DNA only, but a much higher ATPase activity compared to the UvrA/WT-UvrB/UV-DNA reactions.

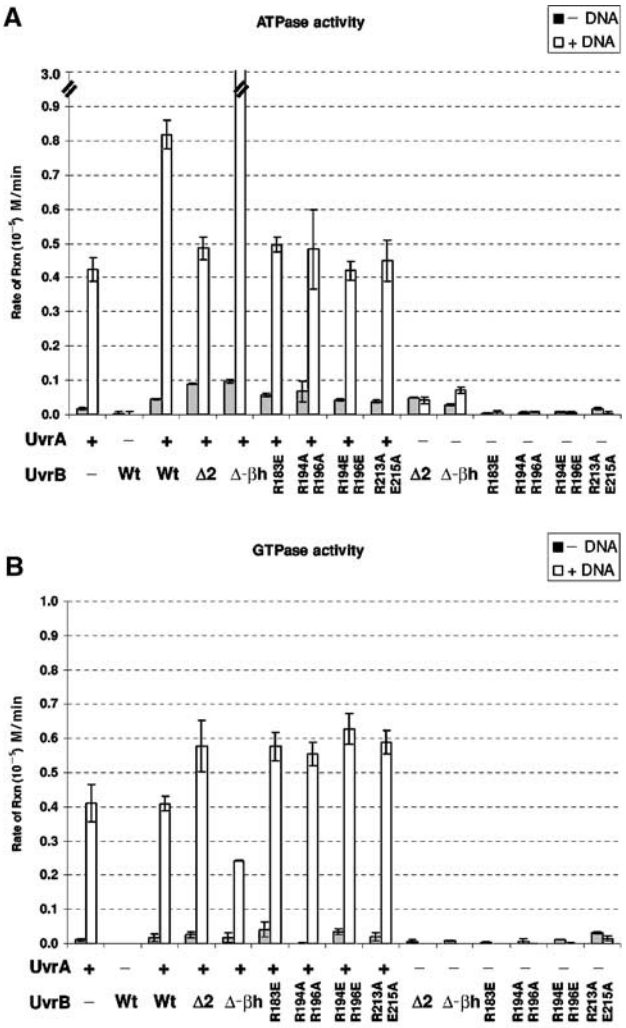


**Figure 8** ATP/GTP hydrolysis by UvrA, WT UvrB or UvrB mutants. (**A**) ATPase activity; (**B**) GTPase activity. Gray bars = hydrolysis of ATP or GTP in the absence of UV-irradiated plasmid DNA (−DNA); white bars = hydrolysis of ATP or GTP in the presence of UV-irradiated plasmid DNA (+DNA). The rate of hydrolysis was calculated from the linear change in $A_{340\,nm}$ over a 30 min period. The rates were determined three times and blank corrected for the oxidation of NADH (+ ATP or GTP) in the absence of the UvrA and UvrB (WT and mutant) proteins. The data are reported as the mean ± the standard error of the mean.

## Discussion

### *Functional role of domain 2*

The UvrB Y96A variant crystallized in a different space group compared to the WT protein, providing the first complete view of domain 2. It was possible to assign all side chains within domain 2, contrary to all previous UvrB structures that lack sequence assignment in this domain. Conserved residues on the surface of domain 2 are in proximity to the β hairpin, which has been proposed to be key in the formation of the pre-incision complex.

To study the functional role of these residues, we have assayed UvrB mutants for their ability to participate in the incision reaction, to form the pre-incision complex, to destabilize short duplex regions in DNA, to bind to UvrA and to hydrolyze ATP. The mutants can be divided into three classes, with R213A/E215A and R194A/R196A showing the mildest defects, R194E/R196E and R183E showing more severe defects and the deletion mutant Δ2 being inactive in all the assays performed. The degree to which UvrB mutants support DNA incision (Figure 4) and duplex destabilization (Figure 7) correlates well with the ability to form a UvrB–DNA pre-incision complex (Figure 6), consistent with the suggestion that formation of the pre-incision complex is the rate-limiting step in UvrABC-mediated excision repair (Van Houten and Snowden, 1993). Pull-down assays with UvrA (Figure 5) indicate that the point mutants of UvrB do not interact as

tightly with UvrA as WT UvrB. However, there is sufficient interaction with UvrA in the presence of DNA (Figure 6) to allow incision to occur at a reduced rate (Figure 4).

### *ATPase/GTPase measurements indicate that all UvrB mutants have altered the crosstalk with UvrA*

UvrA contains two ATPase active sites and their activity is modulated when UvrA binds to undamaged or damaged DNA. In contrast, UvrB contains only one ATPase active site. While UvrB hydrolyzes only ATP, UvrA's ATPase sites can also hydrolyze GTP. By measuring ATPase and GTPase activity side by side, we obtained separate hydrolysis rates for UvrA and UvrB (Figure 8). The ATPase activity of WT UvrB is activated upon binding to UvrA, and is dramatically increased further if damaged DNA is present. This increase of the UvrA/DNA damage-dependent ATPase activity of UvrB is not observed for the domain 2 mutants. The altered ATPase activity of the mutants could be interpreted as evidence that they do not interact with UvrA. However, the incision activity of some of the mutants suggests that at least a transient complex of UvrA, UvrB and damaged DNA forms in the incision assays, which are performed at similar enzyme concentrations as the ATPase assay. Furthermore, recruitment of UvrC by UvrB requires hydrolysis of ATP in the pre-incision complex, that is, after UvrA dissociates, suggesting that these mutants retain ATPase activity. Perhaps the mutations disturb the crosstalk between UvrA and UvrB, leading to a degree of activation and deactivation of UvrA's and UvrB's ATPase activity different from that observed for WT UvrB.

Arg 213 is the only surface residue of domain 2 that is invariant among all the known UvrB and Mfd sequences. The double mutant R213A/E215A retains some activity in the pull-down assay and is almost fully active in the other *in vitro* experiments described. However, mutating this residue alters the ATPase activity of the UvrAUvrB–DNA complex, which might affect the efficiency with which damaged DNA is recognized. In our *in vitro* incision assay, one in 100 nucleotides is damaged, whereas, *in vivo*, damaged DNA has to be detected in the context of a large excess of undamaged DNA. Altering the crosstalk between UvrA and UvrB might decrease the specificity or speed of damage recognition in the context of the cell.

### *How do UvrA and UvrB communicate prior to formation of the incision complex?*

Intriguingly, UvrB lacking either the β hairpin, domain 2 or the C-terminal coiled coil show a low basal ATPase activity (Figure 8 and Hsu *et al*, 1995). Furthermore, the Δβ-hairpin mutant in complex with UvrA exhibits a hyper-ATPase activity, nearly seven times greater than that of UvrA alone. We attribute this hyper-ATPase activity to the fact that the UvrA dimer can recruit the UvrB Δβ-hairpin protein to the lesion, but the defective Δβ-hairpin protein cannot verify the damage and UvrA cannot hand off the DNA to UvrB (Skorvaga *et al*, 2002). Thus, the UvrB mutant hydrolyzes ATP rapidly in an attempt to engage the damage and no incision activity is observed. In contrast, the GTPase activity of UvrA in complex with the Δβ-hairpin mutant is suppressed compared to all other proteins tested. Since the hydrolysis of ATP by the UvrA dimer has been associated with monomerization, the decreased GTPase activity could be attributed to the proteins being 'stuck' in a defective UvrAUvrB complex (the slowly migrating species in lane 9, Figure 6A). This would lend support to our model that the β hairpin binds to the separated DNA strands in the region of the DNA lesion as part of the damage-verification process (Theis *et al*, 2000; Skorvaga *et al*, 2002). In contrast, UvrA's GTPase activity increases in the presence of the UvrB Δ2 mutant and UV-DNA relative to UvrA/UV-DNA only (Figure 8). This increase could be caused by a decrease in stability of the UvrA dimer through the interaction between the C-terminal domain of the Δ2 mutant and UvrA. These results suggest that the β hairpin, domain 2 and the C-terminal coiled coil, are regulators of UvrB's ATPase activity and, through allosteric effects, may also regulate UvrA's ATPase activities.

The β hairpin of UvrB, which has a direct role in damage recognition (Moolenaar *et al*, 2001; Skorvaga *et al*, 2002), presumably changes conformation upon encountering the lesion. The details of the interaction between domain 2 and the remainder of UvrB observed in the structure of UvrB Y96A suggest that structural changes in the β hairpin could cause changes in the position of domain 2 relative to the remainder of the protein, transmitted by conformational changes in the α helix 1a-α4 C terminal to the β hairpin. These events would be sensed by UvrA, which contacts both the DNA and domain 2 of UvrB, and triggers its ATPase activity, causing dissociation from the UvrB–DNA complex. Our results suggest that the strength of the interactions between UvrA and domain 2 of UvrB is critically important for the role of UvrB in damage recognition.

## Conclusion

Structural analysis of the UvrB variant Y96A provided for the first time a detailed view of domain 2. Site-directed mutagenesis of highly conserved residues on the surface, namely Arg 183, Arg 194, Arg 196, Arg 213 and Glu 215, and a complete deletion of this domain indicate that domain 2 plays a critical role in the reaction pathway of nucleotide excision repair. Our results suggest that the strength of the protein–protein interaction between UvrA and domain 2 of UvrB is critically important for the proper functioning of UvrB as a damage recognition component of the UvrABC system. Experiments using site-directed mutants and protein–DNA crosslinking are underway to understand the details of how domain 2 plays its pivotal role in damage recognition and UvrA dissociation, which lead to specific and efficient repair of damaged DNA.

## Materials and methods

### *Expression and purification of the UvrB Y96A variant*

The UvrB point mutant Y96A from *B. caldotenax* was purified using the T7 IMPACT$^{tm}$ system (New England Biolabs) and the protein was expressed in BL21(DE3)RIL cells by standard procedures, followed by gel filtration chromatography (Superdex XK 26/60 column (Pharmacia Biotech)).

### *Crystallization and structure determination*

Crystals of Y96A UvrB were grown by vapor diffusion, equilibrating equal volumes of protein solution (12.5 mg/ml) and precipitant solution containing 16% PEG 6000, 30 mM $ZnCl_2$, 100 mM bicine (pH 9.0), against a reservoir solution containing 20% PEG 6000, 500 mM NaCl and 100 mM Tris–HCl (pH 8.5). The crystals were transferred into precipitant solutions containing increasing amounts of glycerol until a final concentration of 30% was reached, and subsequently cryocooled in liquid nitrogen. Data were collected at

beam line X26C at the National Synchrotron Light Source at Brookhaven National Laboratory, equipped with an ADSC Quantum 4R detector. Diffraction data were processed using the HKL software (Supplementary data). Crystals belong to space group $P3_221$ with $a = 150.8$ Å and $c = 159.8$ Å, and contain two Y96A UvrB molecules per asymmetric unit. The structure was solved by molecular replacement using the program COMO and the structure of UvrB from *B. caldotenax* (PDB code 1D9X) as a search model. Domain 2 (residues 154–247) was rebuilt along with residues 253–299 of domain 1b using the program O. Two-fold noncrystallographic symmetry (NCS) restraints were maintained throughout refinement using REFMAC. TLS refinement was used in the final stages to account for overall anisotropic motion of the molecules. Two TLS groups were defined corresponding to each monomer. The tightness of constraints was chosen to minimize the free *R*-value.

### *Cloning of the Thermotoga maritima uvrC gene*

The *uvrC* gene from *T. maritima* (*Tma*) was amplified by PCR using TmC1 sense, 5′-CACTCCCATATGAAAGAGAAGATCAGAAAGAAGA-3′, TmC2 antisense 5′-TTAGTCACGGCTCTTCCGCACAAAATATC CAGGACCCTTCG-3′ oligonucleotides as primers, *Tma* genomic DNA as template, with *Pfu* DNA polymerase (Stratagene). The PCR conditions were: incubation at 94°C for 3 min; 25 cycles: 94°C for 30 s, 55°C for 30 s, 72°C for 3 min and 30 s, followed by a 10 min incubation at 72°C. The PCR product was column purified (Qiagen), digested with *Nde*I and *Sap*I restriction endonucleases (NEB), isolated from SeaKem agarose and ligated into a pTXB1 vector (NEB). The cloned $uvrC^{Tma}$ gene was sequenced to ensure no mutations.

### *Construction of the UvrB domain 2 mutants*

The construction of single amino-acid residue substitution and deletion mutants of $uvrB^{Bca}$ was performed with the QuickChange Site-Directed Mutagenesis Kit from Stratagene using pUC18$uvrB^{Bca}$ as template, sense and antisense oligonucleotides specific for each mutant as PCR primers, and *Pfu*-ultra DNA polymerase (Stratagene). The sense PCR primers for single mutants are (all the antisense primers are complementary to the sense oligonucleotides; changed nucleotides are shown in bold): R183E mutant, 5′-GACATCCAATACGAC**GAG**AATGACATCGATTTT-3′, R194A/R196A (R194E/R196E) double mutant, 5′-GCCGCGGCACGTT**TGCA**GT**AG CA**(**TGAA**GT**AGAA**)GGCGATGTTGTCGAA-3′, R213A/E215A double mutant, 5′-GATGAACATTGCAT**TGCT**GT**AG**C**G**TTTTTCGGCGAT GAA-3′. The PCR conditions were: incubation at 95°C for 2 min; 25 cycles: 95°C for 30 s, 55°C for 30 s, 72°C for 5 min and 30 s; 1 cycle: 72°C for 10 min.

The PCR primers for the UvrB domain 2 deletion mutant were: 5′-end antisense primer (1: 5′-CCAATTACTAGTTCCCAGTTCGCGG TACTCTTCC-3′) and 3′-end sense primer (2: 5′-AACCTTAC TAGTGGCCCGGCGTCGCACTTCGTGAC-3′). The nucleotides coding for the Gly–Thr–Ser–Gly hinge segment introduced into the deleted sequence between Leu 157 and Pro 245 are underlined. PCR conditions for the Δ2 mutant were: incubation at 95°C for 1 min; 16 cycles: 95°C for 30 s, 55°C for 1 min, 68°C for 10 min and 30 s. Mutagenized *uvrB* inserts were sequenced and subcloned into the pTYB1 vector (NEB).

### *DNA substrates*

DNA substrates were synthesized by Sigma-Genosys (Woodlands, TX). The DNA sequence of the 50mer double-stranded substrate containing a single internal fluorescein (FldT) adduct was: $F_{26}$, 50 (5′-GACTACGTACTGTTACGGCTCCATC[FldT]CTACCGCAATCAGGC CAGATCTGC-3′), while the complementary strand was NDB (5′-GCAGATCTGGCCTGATTGCGGTAGCGATGGAGCCGTAACAGTAC GTAGTC-3′). The $F_{26}$, 50 strand was 5′-end-labeled using T4 polynucleotide kinase and [$^{32}$P]γ-ATP (3000 Ci/mmol, Amersham Biosciences) according to the manufacturer's instructions. The reaction was terminated by the addition of EDTA and the enzyme was heat denatured by incubation for 10 min at 65°C. Unincorporated radioactive nucleotides were removed by gel filtration chromatography (Biospin-6, BioRad). The labeled oligonucleotide was annealed with the complementary oligonucleotide using equimolar amounts. The double-stranded character was analyzed on a native 12% polyacrylamide gel.

For the gapped heteroduplex, the 25mer oligonucleotide MJD1 (5′-GACTACGTACTGTTACGGCTCCATC-3′) was 5′-end-labeled with T4 polynucleotide kinase as described above. The reaction volume was then passed through a Biospin 6 column (pre-washed four times with 10 mM $NH_4OAc$). The column eluent was evaporated to dryness. The 5′-labeled 25mer was resuspended in 1 mM Tris–HCl (pH 7.8)/0.1 mM EDTA and annealed at an equimolar ratio with a 24mer, MJD4 (5′-pCTACCGCAATCAGGCCAGATCTGC-3′, the second half of the top strand) and a 50mer, MJD3 (5′-GCAGATCTGGCCT GATTGCGGTAGCGATGGAGCCGTAACAGTACGTAGTC-3′, bottom strand).

### *UvrABC incision assay*

The 5′-end-labeled duplex DNA (2 nM) was incised by the UvrABC enzymes (20 nM *Bca* UvrA, 50 nM *Tma* UvrC and 100 nM *Bca* UvrB or *Bca* UvrB mutant) in 20 μl of UvrABC buffer (50 mM Tris–HCl (pH 7.5), 50 mM KCl, 10 mM $MgCl_2$, 1 mM ATP and 5 mM DTT) at 55°C for either 5 or 30 min. The reaction was terminated by addition of EDTA (20 mM). In all, 10% of the reaction was removed, denatured with formamide and heated to 85°C for 5 min. Incision products were resolved on a 10% denaturing polyacrylamide gel and electrophoresis was performed at 400 V in Tris–borate–EDTA buffer (1X TBE, 89 mM Tris, 89 mM boric acid and 2 mM EDTA). Gels were dried and exposed to a phosphorimager screen (Molecular Dynamics) overnight. The incision efficiency was calculated using the Molecular Dynamics software ImageQuant.

### *Oligonucleotide-destabilizing assay*

The reaction mixture containing 50 nM *Bca* UvrA, 100 nM *Bca* UvrB (or UvrB mutant) and ~8 fmol (in ssDNA circles) of helicase substrate (M13-F26 oligonucleotide: 5′-TAGATTTAGTT[FldT]GAC CATTAGATACA-3′ annealed to −M13mp19+) in buffer A (50 mM Tris–HCl (pH 7.5), 150 mM KCl, 10 mM $MgCl_2$, 2 mM ATP and 5 mM DTT) was incubated at 42°C for 10 or 30 min, respectively. The reaction was stopped by the addition of 5 μl stop solution (50 v/v glycerol, 1% SDS, 0.1 mM EDTA, 0.25% orange G) and the sample was loaded onto a 12% nondenaturing polyacrylamide gel in Tris–borate–EDTA buffer. Electrophoresis was conducted at 120–150 V for 1–2 h. The gels were analyzed as described above.

### *ATP/GTP hydrolysis assay*

The conversion of ATP to ADP and GTP to GDP by the UvrABC system was monitored using a coupled enzyme assay system consisting of pyruvate kinase and lactate dehydrogenase to link the hydrolysis of ATP or GTP to the oxidation of NADH ($\varepsilon_{340\,nm} = 6220\,M^{-1}\,cm^{-1}$). The assay mixture contained 50 mM Tris–HCl (pH 7.5), 50 mM NaCl, 4 mM $MgCl_2$, 1 mM DTT, 20 U/ml lactate dehydrogenase, 20 U/ml pyruvate kinase, 2 mM phosphoenol pyruvate, 0.15 mM NADH, 100 nM *Bca* UvrA and 50 nM *Bca* UvrB (WT or mutants) in the presence of 10 ng of UV-irradiated DNA substrate. The DNA substrate was prepared by exposure of pUC18 DNA to 200 J/m$^2$. The thermophilic proteins were preheated to 55°C for 10 min prior to adding them to the reaction. The reaction mixture (0.1 ml) equilibrated at 55°C for 5 min followed by the addition of ATP or GTP (0.1 mM). The rate of hydrolysis was calculated from the linear change in the absorbance at 340 nm over a 30 min period, using a Beckman spectrophotometer. The rates were determined three times and blank corrected for the oxidation of NADH (+ATP or GTP) in the absence of the UvrA and/or UvrB proteins. The data are reported as the mean rate (M/min) ± the standard error of the mean.

### *Gel mobility shift assay*

Binding reactions were performed with 2 nM duplexed DNA substrate (5′ $^{32}$P-labeled $F_{26}$, 50), 20 nM *Bca* UvrA and 120 nM UvrB or UvrB mutant in 20 μl UvrABC buffer for 20 min at 55°C. Glycerol was added to the reaction (8% v/v) and the reaction mixture was loaded onto a 4% native polyacrylamide gel (19:1). The gel and the buffer contained 0.5 × TBE with 1 mM ATP and 10 mM $MgCl_2$. Electrophoresis was carried out for 1.5 h at 40 mA and 4°C. The gels were analyzed as described above. Percentage of DNA bound is reported as the mean ± the standard deviation of the mean ($n = 3$).

### *UvrB-pull-down assay*

The plasmid pTYB1 $uvrA^{Bca}$ SD3 N5688 was transformed into Rosetta-gami (DE3) pLacI (Novagen) *E. coli* cells. Overexpression of the *Bca* UvrA protein was induced by the addition of 1 mM IPTG (Gold BioTechnology Inc, MO). Cells were harvested and stored at −80°C. Cell paste from 2 l of culture was resuspended in 40 ml

 

buffer B containing 20 mM Tris (pH 8), 500 mM NaCl, 0.1 mM EDTA, 1 mM PMSF and 0.25% Triton X-100. Cells were lysed in a Branson Sonifier 450 for 5 min twice on ice. The lysate was clarified by centrifugation for 20 min at 10 000 *g*. The supernatant was mixed with 1 ml chitin-binding resin (NEB, MA) and rotated end-over-end for 2 h at 4°C. The lysate-resin slurry was poured into a $1 \times 5$ BioRad column and washed overnight with 200 ml buffer B. The amount of *Bca* UvrA on the beads was determined by boiling the beads in SDS loading buffer and comparing the protein band intensities with those of a known concentration of BSA. The beads contained approximately 1.4 mg of *Bca* UvrA per ml of resin.

The *Bca* UvrA beads (5 µl per sample) were diluted 10-fold with water to reduce the salt concentration to 50 mM NaCl and washed once with buffer C (50 mM Tris–HCl (pH 7.5), 50 mM KCl, 10 mM $MgCl_2$, 1 mM ATP) to remove any unbound *Bca* UvrA. Following centrifugation and removal of the supernatant, the beads were resuspended in buffer C, and 1 µM of the indicated protein in buffer C was added. After 20 min incubation at room temperature, one-twentieth of the reaction was removed and set aside as 'input'. The remaining samples were centrifuged (500 *g*) and the supernatants discarded. The beads were washed three times with buffer C and then resuspended in 2 × NuPage SDS loading buffer, heated to 85°C for 10 min, and loaded onto a precast 10% Tris–Bis gel (Invitrogen). Electrophoresis was performed in MOPS buffer (Invitrogen) for 50 min at 200 V. The gels were removed and stained with Simply Blue Safe Stain (Invitrogen).

***Supplementary data***

Supplementary data are available at *The EMBO Journal* Online.

## Acknowledgements

This research was supported by grants from the DOE grant (DEFG02-01ER63073) and Pew Scholars Program in the Biomedical Sciences to CK. Beamline X26C at the National Synchrotron Light Source in Brookhaven is supported in part by the State University of New York and its Research Foundation. Coordinates will be available from the Protein Data Bank (code 1T5L) and can also be requested from the corresponding authors.

## References

Alexandrovich A, Czisch M, Frenkiel TA, Kelly GP, Goosen N, Moolenaar GF, Chowdhry BZ, Sanderson MR, Lane AN (2001) Solution structure, hydrodynamics and thermodynamics of the UvrB C-terminal domain. *J Biomol Struct Dyn* **19:** 219–236

Boyce RP, Howard-Flanders P (1964) Release of ultra-violet light-induced thymine dimers from DNA in *E. coli* K-12. *Proc Natl Acad Sci USA* **51:** 293–300

Caron PR, Kushner SR, Grossman L (1985) Involvement of helicase-II (UvrD gene product) and DNA polymerase-I in excision mediated by the UvrABC protein complex. *Proc Natl Acad Sci USA* **82:** 4925–4929

Friedberg EC, Walker GC, Siede W (1995) *DNA Repair and Mutagenesis*. Washington, DC: ASM Press

Goosen N, Moolenaar GF (2001) Role of ATP hydrolysis by UvrA and UvrB during nucleotide excision repair. *Res Microbiol* **152:** 401–409

Holm L, Sander C (1995) Dali: a network tool for protein structure comparison. *Trends Biochem Sci* **20:** 478–480

Hsu DS, Kim ST, Sun Q, Sancar A (1995) Structure and function of the UvrB protein. *J Biol Chem* **270:** 8319–8327

Husain I, Houten BV, Thomas DC, Abdel-Monem M, Sancar A (1985) Effect of DNA polymerase I and DNA helicase II on the turnover rate of UvrABC excision nuclease. *Proc Natl Acad Sci USA* **82:** 6774–6778

Koo HS, Claassen L, Grossman L, Liu LF (1991) ATP-dependent partitioning of the DNA template into supercoiled domains by *Escherichia coli* UvrAB. *Proc Natl Acad Sci USA* **88:** 1212–1216

Lin JJ, Phillips AM, Hearst JE, Sancar A (1992) Active site of (A)BC excinuclease: II. Binding, bending and catalysis mutants of UvrB reveal a direct role in 3′ and an indirect role in 5′ incision. *J Biol Chem* **267:** 17693–17700

Lin J-J, Sancar A (1992) Active site of (A)BC excinuclease: I. Evidence for 5′ incision by UvrC through a catalytic site involving $Asp^{399}$, $Asp^{438}$, and $His^{538}$ residues. *J Biol Chem* **267:** 17688–17692

Lloyd RS, Van Houten B (1995) DNA damage recognition. In *DNA Repair Mechanisms: Impact on Human Diseases and Cancer*, Vos J-M (ed), pp 25–66. Austin, TX: R.G. Landes Company, Biomedical Publishers

Machius M, Henry L, Palnitkar M, Deisenhofer J (1999) Crystal structure of the DNA nucleotide excision repair enzyme UvrB from *Thermus thermophilus*. *Proc Natl Acad Sci USA* **96:** 11717–11722

Moolenaar GF, Hoglund L, Goosen N (2001) Clue to damage recognition by UvrB: residues in the beta-hairpin structure prevent binding to non-damaged DNA. *EMBO J* **20:** 6140–6149

Nakagawa N, Masui R, Kato R, Kuramitsu S (1997) Domain structure of *Thermus thermophilus* UvrB protein—similarity in domain structure to a helicase. *J Biol Chem* **272:** 22703–22713

Nakagawa N, Sugahara M, Masui R, Kato R, Fukuyama K, Kuramitsu S (1999) Crystal structure of *Thermus thermophilus* HB8 UvrB protein, a key enzyme of nucleotide excision repair. *J Biochem* **126:** 986–990

Oh EY, Grossman L (1987) Helicase properties of the *Escherichia coli* UvrAB protein complex. *Proc Natl Acad Sci USA* **84:** 3638–3642

Oh EY, Grossman L (1989) Characterization of the helicase activity of the *Escherichia coli* UvrAB protein complex. *J Biol Chem* **264:** 1336–1343

Orren DK, Sancar A (1990) Formation and enzymatic properties of the UvrB–DNA complex. *J Biol Chem* **265:** 15796–15803

Sancar A (1994) Mechanisms of DNA excision repair. *Science* **266:** 1954–1956

Sancar A (1996) DNA excision repair. *Annu Rev Biochem* **65:** 43–81

Sancar A, Rupp WD (1983) A novel repair enzyme: UvrABC excision nuclease of *Escherichia coli* cuts a DNA strand on both sides of the damaged region. *Cell* **33:** 249–260

Selby CP, Sancar A (1993) Molecular mechanism of transcription–repair coupling. *Science* **260:** 53–58

Setlow RB, Carrier WL (1964) The disappearance of thymine dimers from DNA: an error-correcting mechanism. *Proc Natl Acad Sci USA* **51:** 226–231

Skorvaga M, Theis K, Mandavilli BS, Kisker C, Van Houten B (2002) The beta-hairpin motif of UvrB is essential for DNA binding, damage processing, and UvrC-mediated incisions. *J Biol Chem* **277:** 1553–1559

Sohi M, Alexandrovich A, Moolenaar G, Visse R, Goosen N, Vernede X, Fontecilla-Camps JC, Champness J, Sanderson MR (2000) Crystal structure of *Escherichia coli* UvrB C-terminal domain, and a model for UvrB–uvrC interaction. *FEBS Lett* **465:** 161–164

Theis K, Chen PJ, Skorvaga M, Houten BV, Kisker C (1999) Crystal structure of UvrB, a DNA helicase adapted for nucleotide excision repair. *EMBO J* **18:** 6899–6907

Theis K, Skorvaga M, Machius M, Nakagawa N, Van Houten B, Kisker C (2000) The nucleotide excision repair protein UvrB, a helicase-like enzyme with a catch. *Mutat Res* **460:** 277–300

Thiagalingam S, Grossman L (1993) The multiple roles for ATP in the *Escherichia coli* UvrABC endonuclease-catalyzed incision reaction. *J Biol Chem* **268:** 18382–18389

Van Houten B (1990) Nucleotide excision repair in *Escherichia coli*. *Microbiol Rev* **54:** 18–51

Van Houten B, Snowden A (1993) Mechanism of action of the *Escherichia coli* UvrABC nuclease: clues to the damage recognition problem. *BioEssays* **15:** 51–59

Verhoeven EE, Wyman C, Moolenaar GF, Goosen N (2002) The presence of two UvrB subunits in the UvrAB complex ensures damage detection in both DNA strands. *EMBO J* **21:** 4196–4205

Verhoeven EEA, van Kesteren M, Moolenaar GF, Visse R, Goosen N (2000) Catalytic sites for 3'- and 5′ incision of *E. coli* excision repair are both located in UvrC. *J Biol Chem* **275:** 5120–5123

Zou Y, Liu T, Geacintov NE, Van Houten B (1995) Interaction of the UvrABC nuclease system with a DNA duplex containing a single stereoisomer of dG-(+)- or dG-(−)-anti-BPDE. *BioChemistry* **34:** 13582–13593